

# Relationship between solar wind, $D_{st}$ , and plasmasphere trough mass density on one-hour time scales

Victoir Veibell\* R.S. Weigel†

February 25, 2016

---

## Abstract

This paper compares various magnetosphere conditions around the onset of geomagnetic events, defined as decreases in  $D_{st}$  below a threshold value or  $\rho_{eq}$  above a threshold value.

**More detail**

## 1 Introduction

Gallagher et al. [1988] **Too far back?** first models the the plasmasphere as a simple linear fit dependent on L shell, geographic height, geomagnetic latitude, and  $K_p$ . Hamilton et al. [1988] simultaneously analyzes a strong geomagnetic storm by comparing empirical energy measurements of the ring current to  $D_{st}$ , along with measuring ring current compositions before, during, and after the storm.

Loto'aniu et al. [1999] uses CRRES to compare in-situ measured plasma mass density to that inferred by ground-based ULF wave measurements extended to the plasmatrough.

Takahashi et al. [2006] estimated magnetospheric mass density using measurements from the CRRES satellite during a 73-day period in 1991 and found that the average ion mass,  $M = \rho/n_e$ , correlated with geomagnetic activity, with more negative  $D_{st}$  values corresponding to slightly higher average ion mass densities. They also found a relationship between the average ion mass and 1.5- and 3-day averages of  $K_p$ , with an increasing correlation as  $K_p$  was smoothed to longer timescales. The CRRES measurements used occurred in the MLT range of 12:00 and 18:00 mostly in the plasma trough (between  $2-7R_E$ ) on an elliptical, nearly equatorial orbit.

Takahashi et al. [2010] developed a mass density dataset using measurements from the GOES satellites

over the years 1980 through 1992, with most measurements in the range  $L = 6.8 \pm 0.2R_E$ . The mass density  $\rho$  was estimated using the the Alfven wave velocity relationship,  $V_A = B/\sqrt{\mu_0\rho}$ , a magnetic field model, and a numerical solution to a wave equation with an ionospheric boundary and the assumption of a zero resistance ionosphere. The equatorial mass density,  $\rho_{eq}$ , was derived from the estimated mass density using a power law dependence on the geocentric distance to the field line of the observation,  $R$ ,  $\rho = \rho_{eq}L/(R/R_E)$ .

Takahashi et al. [2010] **Necessary repetition?** noted that downward spikes in the  $D_{st}$  index coincide with significant changes in  $\rho_{eq}$  at an L-shell of  $6.8 R_E$ . For five storms over a 20-day period, two had  $\rho_{eq}$  spikes after the  $D_{st}$  drop, two had  $\rho_{eq}$  spikes before the drop, and one showed little change in  $\rho_{eq}$ . A key result was that when daily-averaged measurements were considered, an enhancement in  $\rho_{eq}$  appeared on the same day as minimum  $D_{st}$ , indicating the possibility of a solar wind control over  $\rho_{eq}$ .

The results of Takahashi et al. [2006] and Takahashi et al. [2010] are consistent with other results on changes in mass density in the plasma trough region. Yao et al. [2008] studied the relationship between  $D_{st}$  and ion number density for different ion species in different regions (ring current and plasma sheet) and found a general correlation during each of the four storms considered.

---

\*vveibell@gmu.edu

†rweigel@gmu.edu

## 2 Data Preparation

The parameters  $\rho_{eq}$  and  $F_{10.7}$  used in this work are from the dataset associated with Denton [2007], with data available from 1980 through 1991; all other parameters are from Kondrashov et al. [2014] over the time range of 1972 through 2013, which are on a 1-hour time grid.  $\rho_{eq}$  is the inferred equatorial mass density based on the 3rd harmonic toroidal frequency of magnetic field measurements. The smallest cadence for  $\rho_{eq}$  values is 10 minutes. To compute an hourly average over the same interval for which the solar wind parameters were averaged, the median of all  $\rho_{eq}$  values in a given hourly range was used. Fill values were used for hours in which no measurements were available. In cases where  $\rho_{eq}$  was available from multiple Geostationary Operational Environmental Satellites (GOES) satellites at the same time in the Denton [2007] dataset, the value from GOES 6 was selected. In the dataset, measurements from GOES 6 had the longest time span of coverage. An overview of the data is shown in Figure 1.

In this work, events defined to occur when  $D_{st}$  or  $\rho_{eq}$  crosses a threshold value, as indicated in by horizontal dashed lines in the respective panels of Figure 1. In finding  $\rho_{eq}$  events, all fill values were replaced with linearly interpolated values.

## 3 Results

Figure 1 shows values of solar wind averages and mass density used in this study.

Figure 2 shows the long-term trends of  $\log(\rho_{eq})$  and  $F_{10.7}$  computed using the median values in 27-day (non-overlapping?) windows using all non-fill hourly values. A scatter plot of these two lines is shown in Figure 2. The linear correlation is found to be 0.94 matching the value found by Takahashi et al. [2010] who used measurements from all satellites in the time interval of 1980 through 1991.

### 3.1 $D_{st}$ and $\rho_{eq}$ Events

Two types of events are considered. The first is a drop in  $D_{st}$  below the threshold of  $-50$  nT. The second is an increase in  $\rho_{eq}$  above  $40$  amu/cm<sup>3</sup>.

Our first analysis uses data only from the time interval 1989-1991. For both types of events, the hour of the threshold crossing defines the zero epoch time, and for each event  $8 \cdot 24$  hours were kept after each event and  $4 \cdot 24$  hours before each event. To compute the epoch averages on a daily time scale, the median value of all measurements for all events centered on a

window of  $\pm 12$  hours was computed, and these windows were shifted in increments of 24 hours. (Similar results are obtained if we first reduce each event time series to have a 1-day cadence by computing medians in 1-day bins and then compute the medians accross events.) Error bars for each parameter were computed using the standard deviation of the number of values used in computing the median divided by the square root of the number of values used.

In the upper panel of 3,  $D_{st}$  events are shown. The minimum  $D_{st}$  median is  $-48$  nT. Consistent with Takahashi et al. [2010],  $D_{st}$  events correspond to elevated  $\rho_{eq}$ , although the magnitude of increase observed here is  $\sim 2$  amu/cm<sup>3</sup> instead of the value of  $\sim 10$  amu/cm<sup>3</sup> found in Takahashi et al. [2010]. The vertical green bars in the  $\rho_{eq}$  plot show the number of  $\rho_{eq}$  values that were used to compute its median and error bars. Note that for  $D_{st}$ , the number of measurements used in computing the medians is much larger as we use all available  $D_{st}$  measurements instead of restricting to only values where a non-fill  $\rho_{eq}$  value existed.

In the lower panel of 3 it is shown that all trends seen in the analysis of 1989-1991 also hold for the entire run of GOES 6 over 1983-1991, including the magnitude of change in  $\rho_{eq}$  across event onset.

It was found that  $\rho_{eq}$  enhancements do not clearly correspond to a signature in  $D_{st}$ , but that there is a trend for such enhancements to occur when  $B_z$  in the IMF is positive. This is consistent with Takahashi et al. [2010] who note that very large increases in  $\rho_{eq}$  often corresponded to movement of the plasmasphere to beyond geosynchronous distances.

This method finds 669 such periods between May 1983 and August 1991 with an average duration of 9 hours and a median duration of 3 hours. Figure 4 shows the average values of all events over a window of 24 hours before onset and 48 hours after. Figure 4a shows events selected by looking for event onsets where  $D_{st}$  crossed a threshold of  $-40$  nT. The dashed red lines indicate plus and minus one standard deviation of values from all events that went into the average. The final plot in the stack shows both  $\rho_{eq}$  and a bar plot of how many valid data points went into the  $\rho_{eq}$  average. Since  $\rho_{eq}$  comes from a sparser dataset, it has less valid points contributing to the averages than the other parameters in the stack. A subset of longer duration events will be looked at later.

This figure shows a definite spike in the  $Z$  component of the magnetic field, as well as the defined drop in  $D_{st}$ , but no obvious change in mass density at an hourly timescale. This points to an issue with only looking at long-timescale trends between density and  $D_{st}$ , and allows for the possibility that other factors are influencing the long term correlation since there's no obvious connection on a short timescale. One possibility is that, as suggested in [Takahashi et al. \[2010\]](#),  $F_{10.7}$  plays a significant role in driving long term density values which biases the long term correlation of density and  $D_{st}$ .

Two types of events are considered. The first is a drop in  $D_{st}$  below the threshold of  $-40$  nT. The second is an increase in  $\rho_{eq}$  above  $40$  amu/cm<sup>3</sup>.

Our first analysis uses data only from the time interval 1989-1991. In this interval, there were (?)  $D_{st}$  events and (?)  $\rho_{eq}$  events. For both types of events, the hour of the threshold crossing defines the zero epoch time, and for each event  $8 \cdot 24$  hours were kept after each event and  $4 \cdot 24$  hours before each event. To compute the epoch averages on a daily time scale, the median value of all measurements for all events centered window of  $\pm 12$  hours was computed, and these windows were shifted in increments of 24 hours. (Similar results are obtained if we first reduce each event time series to have a 1-day cadence by computing medians in 1-day bins and then compute the medians accross events.) Error bars for each parameter were computed using the standard deviation of values used in computing the median divided by the square root of the number of values used.

In the upper panel of [3](#),  $D_{st}$  events are shown. The minimum  $D_{st}$  median is  $-48$  nT. Consistent with [Takahashi et al. \[2010\]](#),  $D_{st}$  events correspond to elevated  $\rho_{eq}$ , although the magnitude of increase observed here is on the order of  $\sim 2$  amu/cm<sup>3</sup> instead of  $\sim 10$  amu/cm<sup>3</sup> found in [Takahashi et al. \[2010\]](#). The vertical green bars in the  $\rho_{eq}$  plot show the number of  $\rho_{eq}$  values that were used to compute its median and error bars. Note that for  $D_{st}$ , the number of measurements used in computing the medians is much larger as we use all available  $D_{st}$  measurements instead of restricting to only values where a non-fill  $\rho_{eq}$  value existed.

In the lower panel of [3](#),  $\rho_{eq}$  events are shown. Here we see that  $\rho_{eq}$  enhancements do not clearly correspond to a signature in  $D_{st}$ , but that there is a trend for such enhancements to occur when  $B_z$  in the IMF is positive. This is consistent with [Takahashi et al.](#)

[\[2010\]](#) who note that very large increases in  $\rho_{eq}$  often corresponded to movement of the plasmasphere to beyond geosynchronous distances.

A total of 668 events were found in the interval of May 1983 through August 1991 with an average duration of 9 hours and a median duration of 3 hours. Figure [4](#) shows the average values of all events over a window of 24 hours before onset and 48 hours after. Figure [4a](#) shows events selected by looking for event onsets where  $D_{st}$  crossed a threshold of  $-50$  nT. The dashed red lines indicate plus and minus one standard deviation of values from all events that went into the average. The final plot in the stack shows both  $\rho_{eq}$  and a bar plot of how many valid data points went into the  $\rho_{eq}$  average. Since  $\rho_{eq}$  comes from a sparser dataset, it has less valid points contributing to the averages than the other parameters in the stack. A subset of longer duration events will be looked at later.

This figure shows a definite spike in the  $Z$  component of the magnetic field, as well as the defined drop in  $D_{st}$ , but no obvious change in mass density at an hourly timescale. This points to an issue with only looking at long-timescale trends between density and  $D_{st}$ , and allows for the possibility that other factors are influencing the long term correlation since there's no obvious connection on a short timescale. One possibility is that, as suggested in [Takahashi et al. \[2010\]](#),  $F_{10.7}$  plays a significant role in driving long term density values which biases the long term correlation of density and  $D_{st}$ .

## 4 More specific events

It's hypothesized that progressively picking more specific event criteria will allow for the possibility of more significant results, at the expense of more bias in the selection process and potentially less overall usefulness of the results. That said, the predictability of extreme events is of definite interest, so an attempt has been made to find some reproducible method of prediction. Looking at events that last longer than 12 hours and events with an onset threshold less than  $-80$  nT finds both result in a spike in mass density, but also a definite lack of data availability to the point where that spike may be coming from less than five of the total 211 events.

### 4.1 Change in $\rho_{eq}$

Instead of looking for events based on a threshold of  $D_{st}$ , we instead looked for a certain amount of change in  $\rho_{eq}$  as the basis for event onset. Both raw change and percent change were done in case of

bias towards high or low  $\rho_{eq}$  periods, respectively, but neither showed any correlation to a change in  $D_{st}$ .

## 5 F10.7 dependence

In an effort to analyze the dependence of  $\rho_{eq}$  on  $F_{10.7}$ , a few tests were performed. [Takahashi et al. \[2010\]](#) mention a strong correlation between the two. The long term correlation could be a bias for  $D_{st}$ 's effects, so a linear model was created, recreating mass density purely from  $F_{10.7}$  in the form of  $\rho_{eq}(t) = a \cdot F_{10.7}(t)$ . This re-created  $\rho_{eq}$  shows around a 45% correlation with the actual  $\rho_{eq}$ , suggesting a strong influence, while doing the same procedure with  $D_{st}$  shows only a 20-25% correlation.

Figure 5 takes the events and bins them by the value of  $F_{10.7}$  at event onset, then looks at both  $\rho_{eq}$  and  $B_z$ . Error bars calculated in the same manner as before are added to the highest and lowest bins. A significant difference is seen in  $\rho_{eq}$  between events taking place during periods of high  $F_{10.7}$  and low  $F_{10.7}$ , while a much less significant, but still noticeable, difference is seen in  $B_z$ . Also of interest is how  $\rho_{eq}$  only sharply reacts to  $D_{st}$  events during periods of high  $F_{10.7}$ . The positive relationship seen in [Takahashi et al. \[2010\]](#) could be due to the short time period looked at, and that it coincides with periods of higher  $F_{10.7}$ .

Looking at GOES 2,5,6, and 7 shows that this post-onset  $D_{st}$  spike happens in almost every case for periods of high  $F_{10.7}$ . Creating a linear model directly relating variables (and combinations of variables) to  $\rho_{eq}$  also shows that  $F_{10.7}$  most often has the highest correlation with  $\rho_{eq}$ . A sample of these correlations is shown in Table 1. The correlations were made by training a one-input linear model of 5-hour post-onset medians of each variable (or variables) against the median of  $\rho_{eq}$  at, and four hours after, event onset. This was done by randomly sampling half of the data, generating the model, and testing against the other half, doing this process 100 times and then taking the median correlations.

## 6 Appendix

### 6.1 Bias

While attempting to reproduce Figure 11 from [Takahashi et al. \[2010\]](#), an ambiguity in data-handling was found. It is unknown how they got from hourly  $\rho_{eq}$  to daily medians, whether in one step or two steps, and whether the hourly medians are an hour ahead of each hour grid point, or a median of points a half hour to either side, so attempts were

	GOES 2	GOES 5	GOES 6	GOES 7
doy	-0.08	+0.10	-0.05	+0.06
MLT	-0.09	-0.09	-0.04	-0.05
Bz	+0.17	-0.12	+0.08	-0.08
Vsw	-0.04	+0.29	+0.06	-0.06
Dst	+0.27	+0.66	+0.06	+0.22
Rhosw	+0.34	+0.63	+0.07	+0.34
F107	+0.42	+0.14	+0.49	+0.42
Bz+Vsw	+0.09	+0.19	+0.12	-0.11
Dst+F107	+0.45	+0.69	+0.53	+0.47
All	-0.10	+0.34	+0.61	+0.39

Table 1: Table of linear model correlations showing the median of 100 random samples. Each sample trained on half of the data (via randomly selected rows of the least squares matrix) and tested on the other half

made to reproduce all possibilities and compare in order to find a data-handling method with the least bias. These attempts are shown in Figure ?? . This also shows the effect of only considering events with a minimum before noon. All show a similar spike in  $\rho_{eq}$  at the time of  $D_{st}$  minimum, though none quite reproduce the exact values seen in [Takahashi et al. \[2010\]](#). Figure ?? shows where the median falls for all of the found events during that period, as a sanity check for why the prior work would get median values nearing 30 amu/cm<sup>3</sup>. Both authors of this paper conducted independent trials to confirm that the data and analysis don't quite yield the results of Figure 11 in [Takahashi et al. \[2010\]](#) with the processes described in that paper, but the same general trend is still seen.

To check for potential bias in the data as used by our analysis, we checked how the data availability varied with hour, shown in Figure ?? . We also looked at how storm conditions affected data availability. Both a two sample t-test for difference in means and a Wilcoxon rank sum test showed significance at the 1% level that  $D_{st}$  during periods with available data was of a different distribution than  $D_{st}$  during periods missing data. When testing for other significant  $D_{st}$  differences, the Wilcoxon test was significant while the t-test was not in pre-noon vs post-noon distributions, as well as  $\rho_{eq} > 40$  vs  $\rho_{eq} < 40$  distributions indicating perhaps an increase in variability without an increase in mean.

While the GOES Satellites tend to keep an average geostationary distance of around  $L = 6.8R_E$  shown in [Takahashi et al. \[2010\]](#), the actual plasmopause location varies significantly, as shown in [O'Brien and](#)

Moldwin [2003]. This means that during periods of large  $D_{st}$  the plasmopause may be far from the point of measurement of  $\rho_{eq}$  creating a discord in the correlation. Gallagher et al. [2000] provides a model for  $\rho_{eq}$  at a range of L-shells and a brief discussion of the elemental contributions.

## References

- R. Denton. Database of Input Parameters for Tsyganenko Magnetic Field Models, 2007. URL <http://www.dartmouth.edu/~rdenton/magpar/index.html>.
- D. L. Gallagher, P. D. Craven, and R. H. Comfort. An empirical model of the earth's plasmasphere. *Advances in Space Research*, 8:15–21, 1988. doi:[10.1016/0273-1177\(88\)90258-X](https://doi.org/10.1016/0273-1177(88)90258-X).
- D. L. Gallagher, P. D. Craven, and R. H. Comfort. Global core plasma model. *Journal of Geophysical Research*, 105:18819, August 2000. doi:[10.1029/1999JA000241](https://doi.org/10.1029/1999JA000241).
- D. C. Hamilton, G. Gloeckler, F. M. Ipavich, B. Wilken, and W. Stuedemann. Ring current development during the great geomagnetic storm of February 1986. *J. Geophys. Res.*, 93:14343–14355, December 1988. doi:[10.1029/JA093iA12p14343](https://doi.org/10.1029/JA093iA12p14343).
- D. Kondrashov, R. Denton, Y. Y. Shprits, and H. J. Singer. Reconstruction of gaps in the past history of solar wind parameters. *Geophysical Research Letters*, 41:2702–2707, April 2014. doi:[10.1002/2014GL059741](https://doi.org/10.1002/2014GL059741).
- T. M. Loto'aniu, C. L. Waters, B. J. Fraser, and J. C. Samson. Plasma mass density in the plasmatrough: Comparison using ULF waves and CRRES. *Geophys. Res. Lett.*, 26:3277–3280, 1999. doi:[10.1029/1999GL003641](https://doi.org/10.1029/1999GL003641).
- T. P. O'Brien and M. B. Moldwin. Empirical plasmopause models from magnetic indices. *Geophysical Research Letters*, 30:1152, February 2003. doi:[10.1029/2002GL016007](https://doi.org/10.1029/2002GL016007).
- K. Takahashi, R. E. Denton, R. R. Anderson, and W. J. Hughes. Mass density inferred from toroidal wave frequencies and its comparison to electron density. *Journal of Geophysical Research (Space Physics)*, 111:A01201, January 2006. doi:[10.1029/2005JA011286](https://doi.org/10.1029/2005JA011286).
- K. Takahashi, R. E. Denton, and H. J. Singer. Solar cycle variation of geosynchronous plasma mass density derived from the frequency of standing Alfvén waves. *Journal of Geophysical Research (Space Physics)*, 115:A07207, July 2010. doi:[10.1029/2009JA015243](https://doi.org/10.1029/2009JA015243).
- Y. Yao, K. Seki, Y. Miyoshi, J. P. McFadden, E. J. Lund, and C. W. Carlson. Effect of solar wind variation on low-energy O<sup>+</sup> populations in the magnetosphere during geomagnetic storms: FAST observations. *Journal of Geophysical Research (Space Physics)*, 113, 2008. doi:[10.1029/2007JA012681](https://doi.org/10.1029/2007JA012681).

## 7 Figures

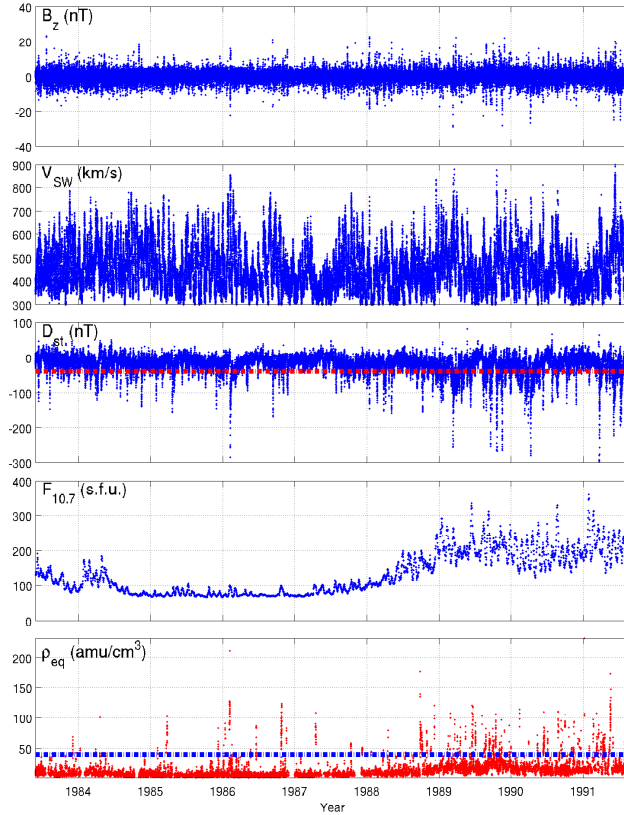


Figure 1: Overview of data used in this study. The top four panels show parameters from Kondrashov et al. [2014] and the bottom panel is based on  $\rho_{eq}$  from Denton [2007] after interpolation and averaging described in the text. Dashed horizontal lines in the  $D_{st}$  and  $\rho_{eq}$  panels indicate sample event cutoff thresholds of  $D_{st} = -50$  nT and  $\rho_{eq} = 40$  amu/cm<sup>3</sup>

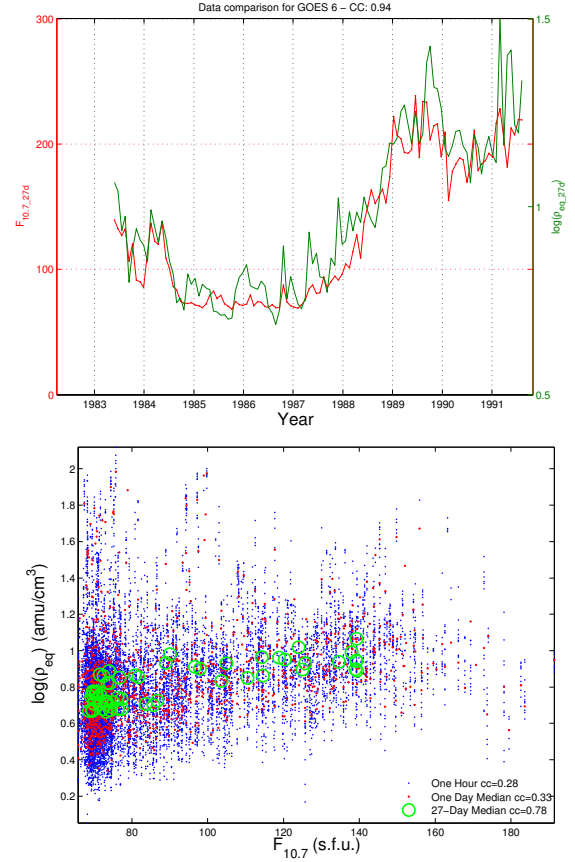


Figure 2: (a) 27-day averages of  $F_{10.7}$  and  $\rho_{eq}$ . (b) Correlation between  $\log(\rho_{eq})$  and  $F_{10.7}$  using hour, day, and 27-day averaging intervals; compare to Takahashi et al. [2010] Fig. 14.



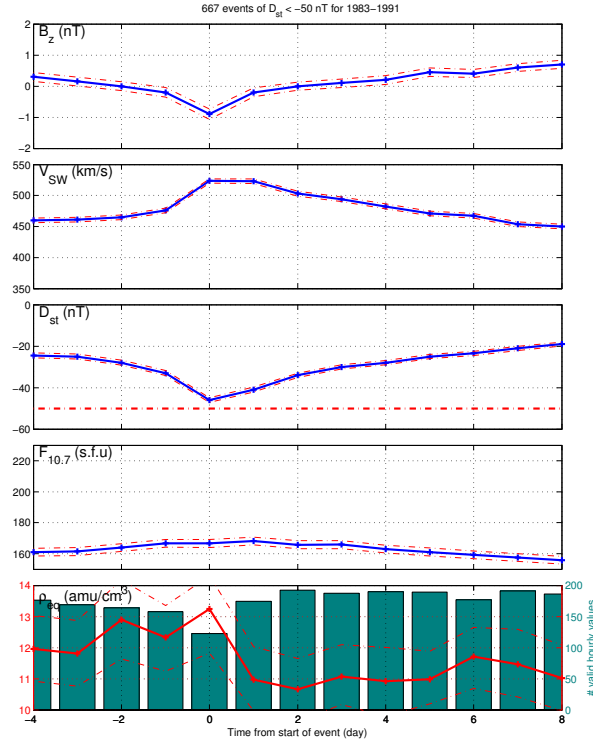
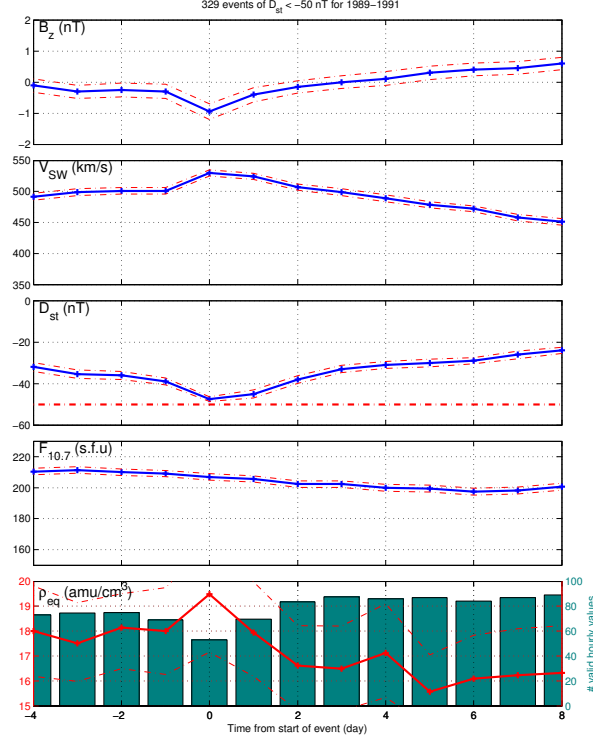


Figure 3: Events in the interval 1989-1991. Upper panel:  $D_{st}$  events. Lower panel: Events in the interval 1983-1991.

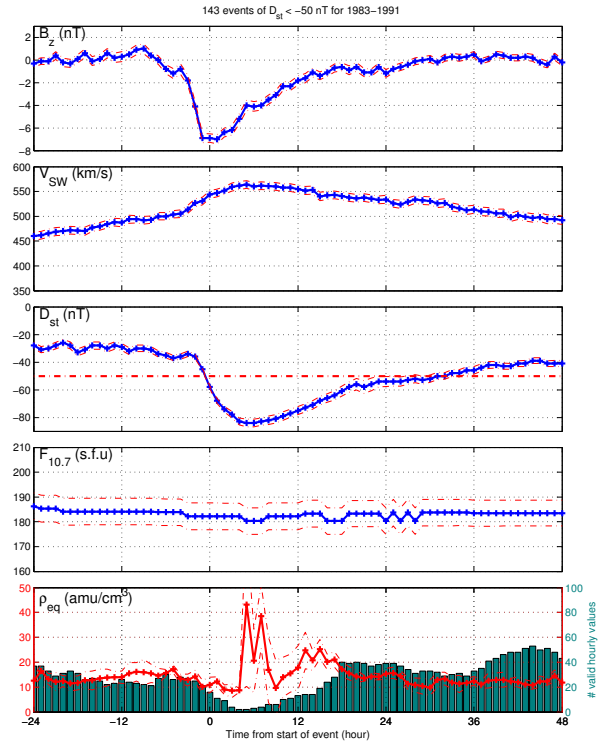
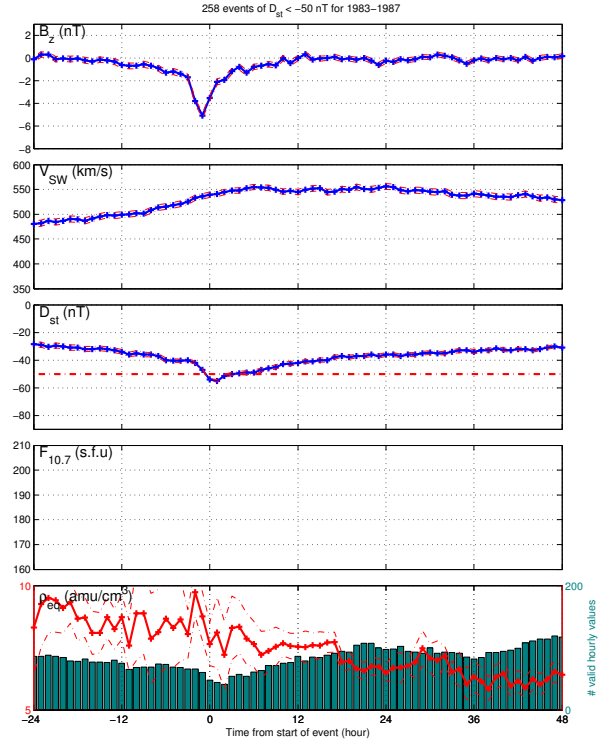


Figure 4: (a) Average of solar wind and near-Earth measurements around the time  $D_{st}$  crossed below  $-50$  nT onset. (b) Same as (a) except for constraint that  $D_{st}$  stayed below  $-50$  nT for at least 12 hours.

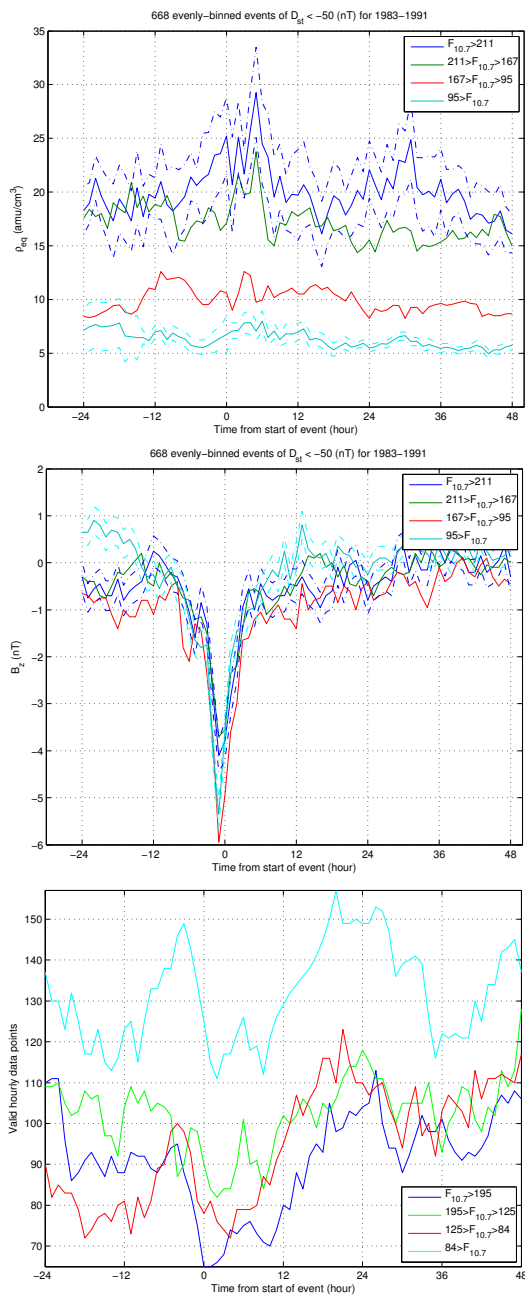


Figure 5: Binning events by  $F_{10.7}$  value at onset for  $\rho_{eq}$  and, in the middle panel,  $B_z$ . Lower panel shows number of valid points in each bin



## 8 Appendix

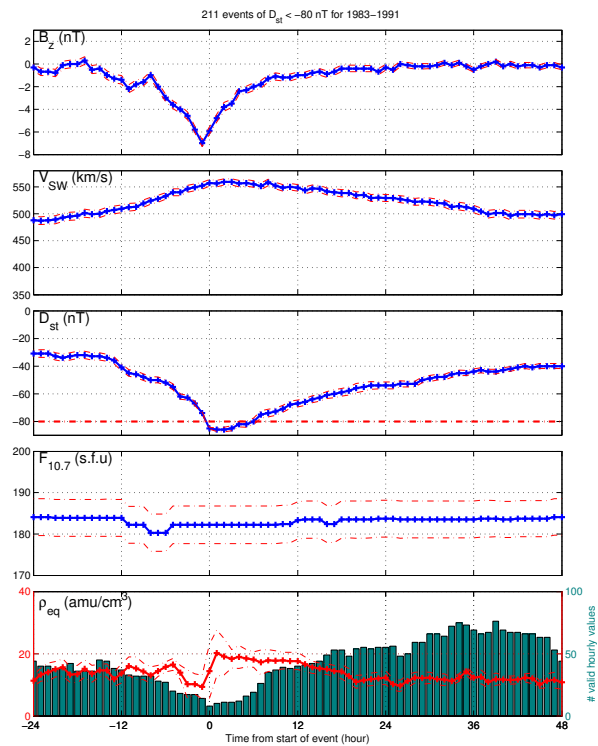


Figure 6: (a) Same as Figure 4(a) except with constraint that  $D_{st}$  crossed below  $-80$  nT

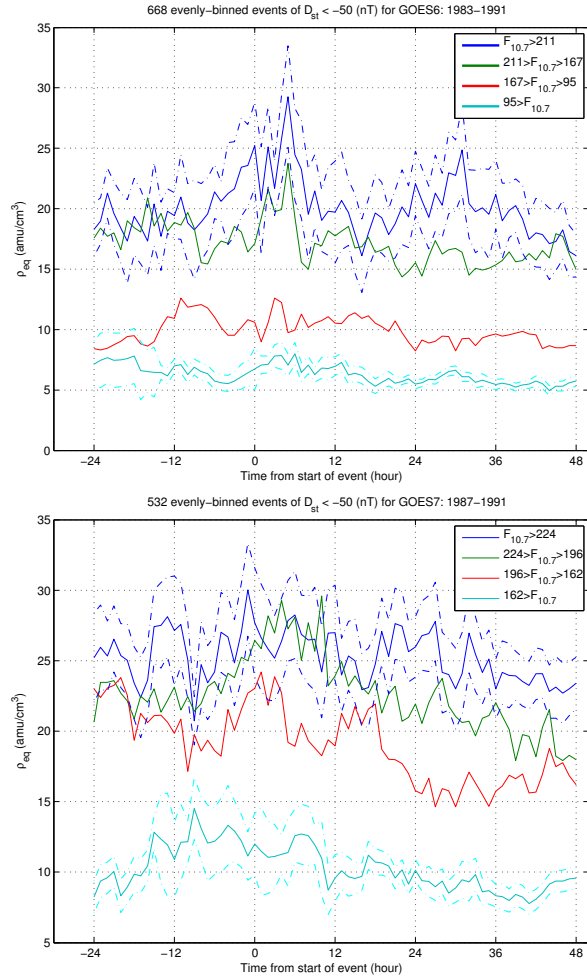


Figure 7: GOES Satellite 6 and 7

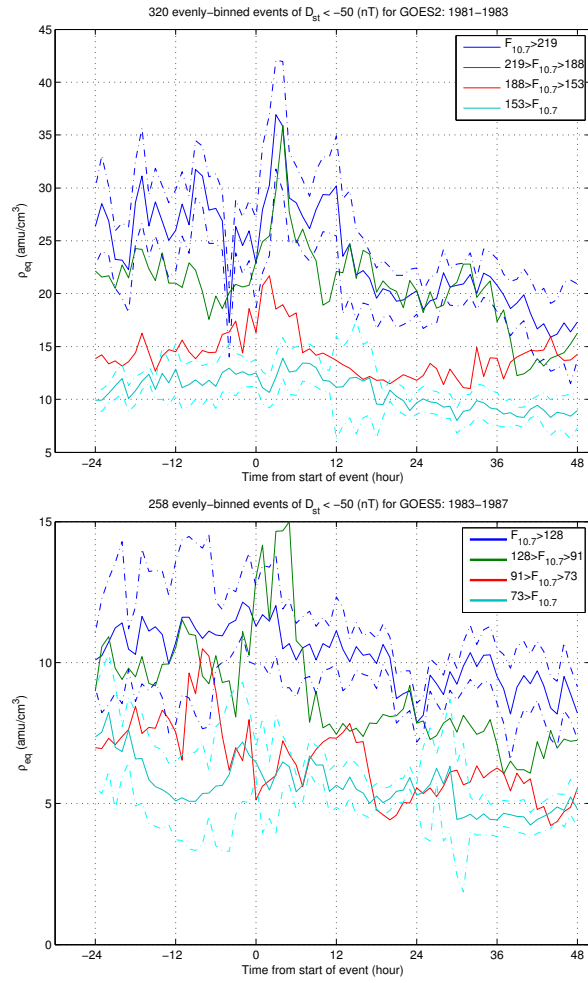


Figure 8: GOES Satellite 2 and 5

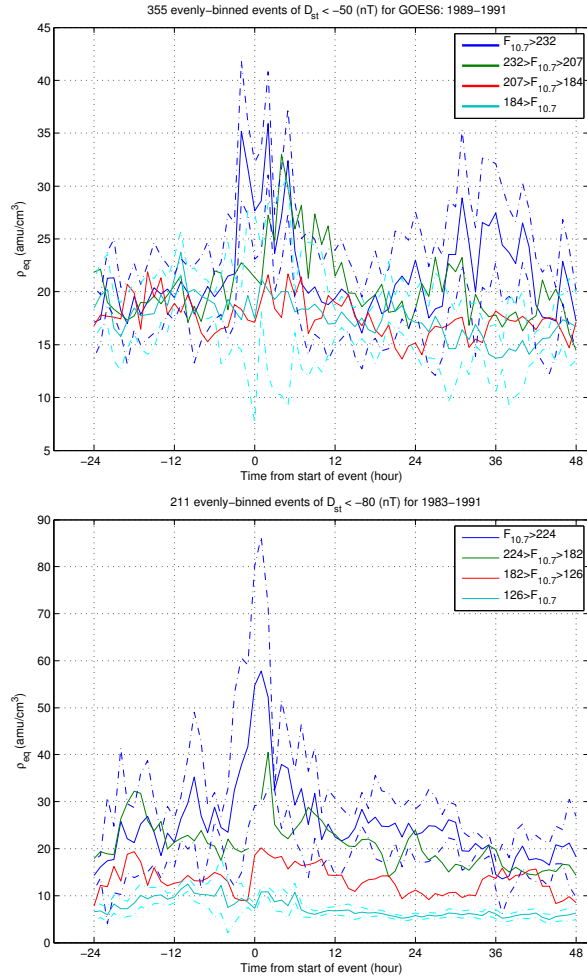


Figure 9: Top: GOES 6 from 89-91 (compare to Takahashi 2010). Bottom:  $D_{st} < -80$  nT.

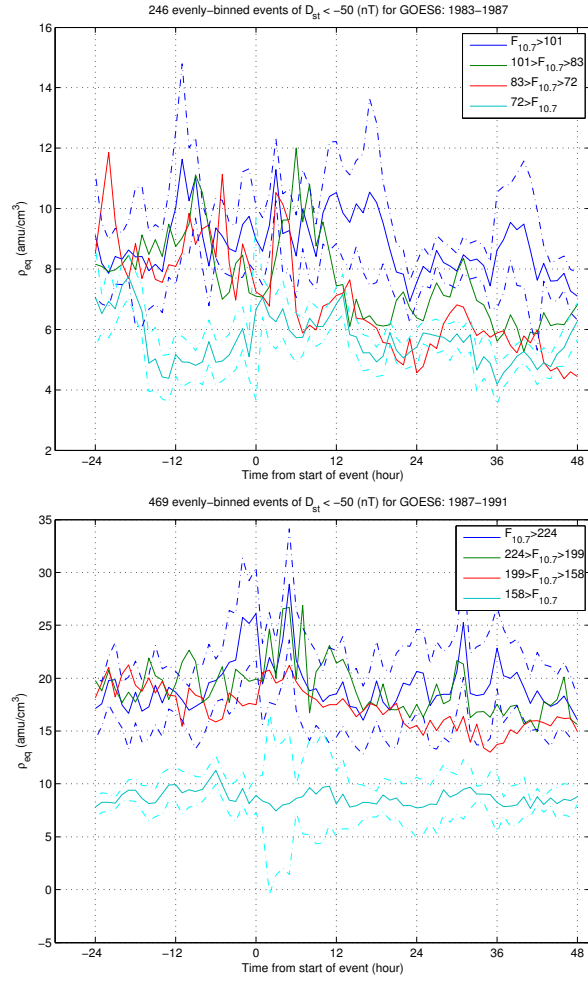


Figure 10: GOES 6 from 83-87 and 87-91

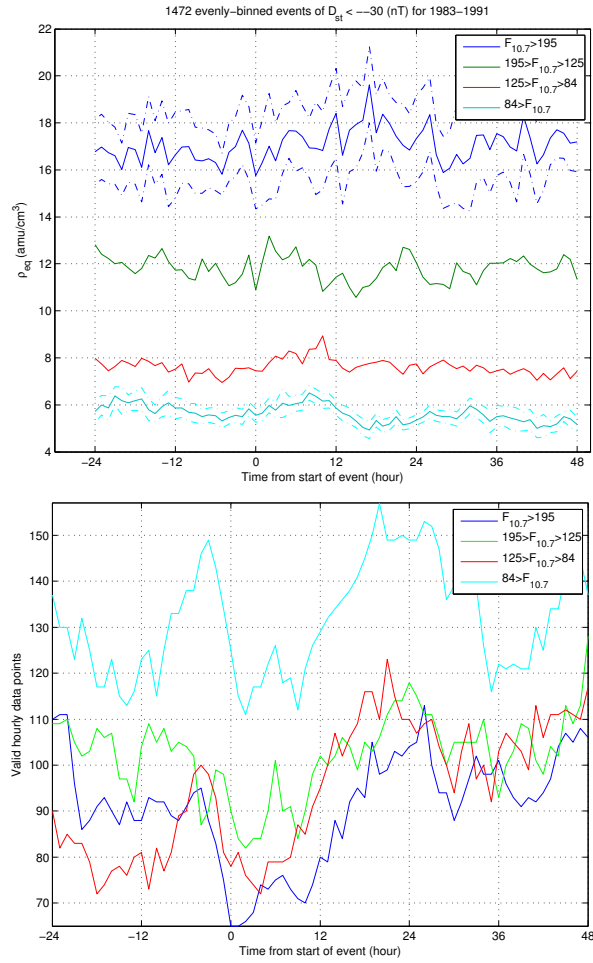


Figure 11:  $D_{st} < -30$  nT events,  $\rho_{eq}$  binned by  $F_{10.7}$ . Lower panel: valid hourly points

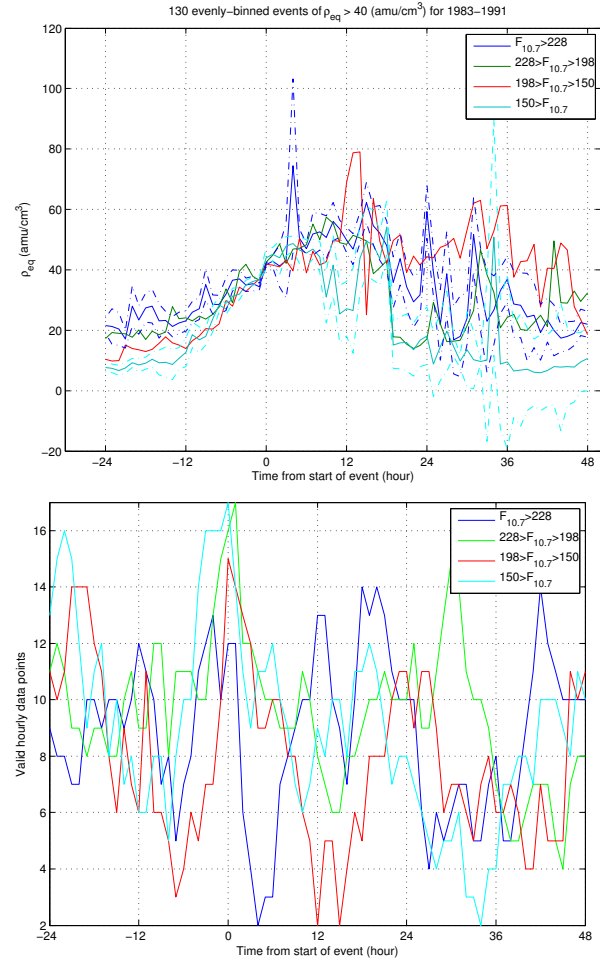


Figure 12:  $\rho_{eq} > 40$  amu/cm<sup>3</sup> events,  $\rho_{eq}$  binned by  $F_{10.7}$

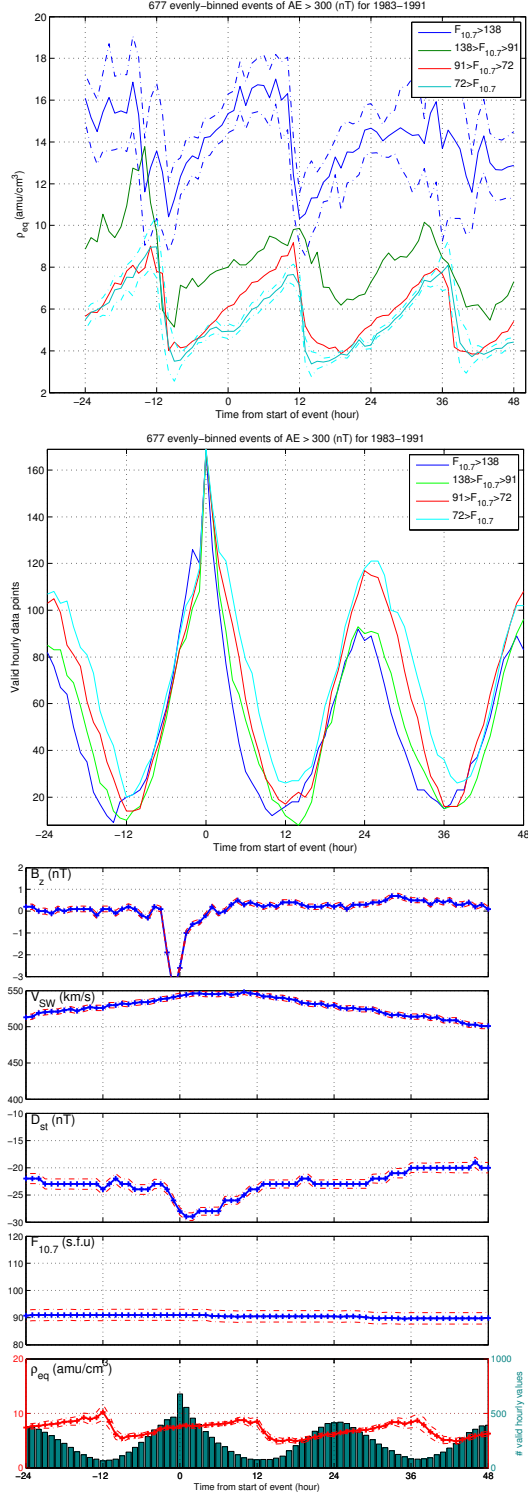


Figure 13: Top:  $AE > 400$  nT events,  $\rho_{eq}$  binned by  $F_{10.7}$  Bottom: averages of  $AE > 400$  events

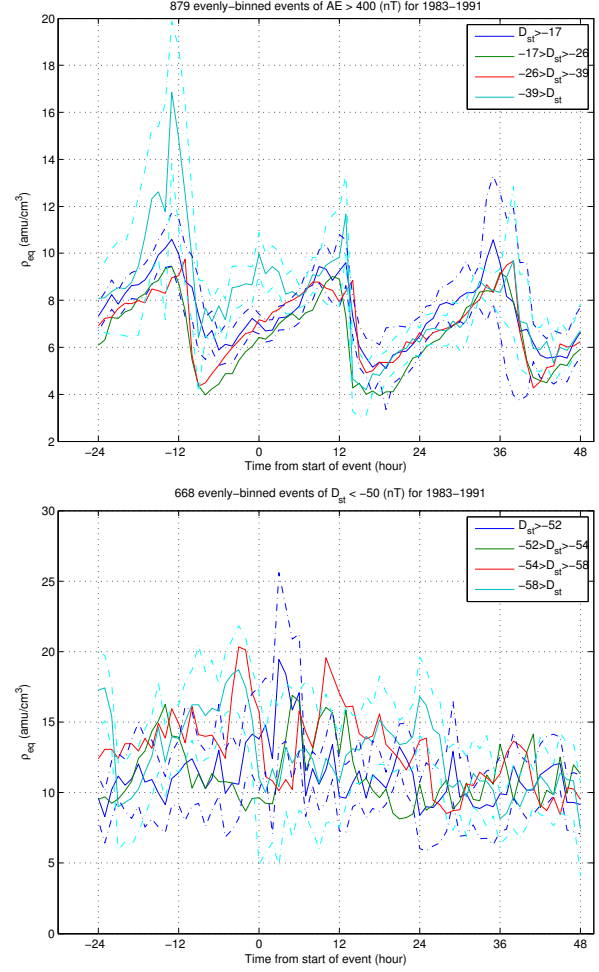


Figure 14: Top:  $AE > 400$  nT events. Bottom:  $D_{st} < -50$  nT events. Both  $\rho_{eq}$  binned by  $D_{st}$ .

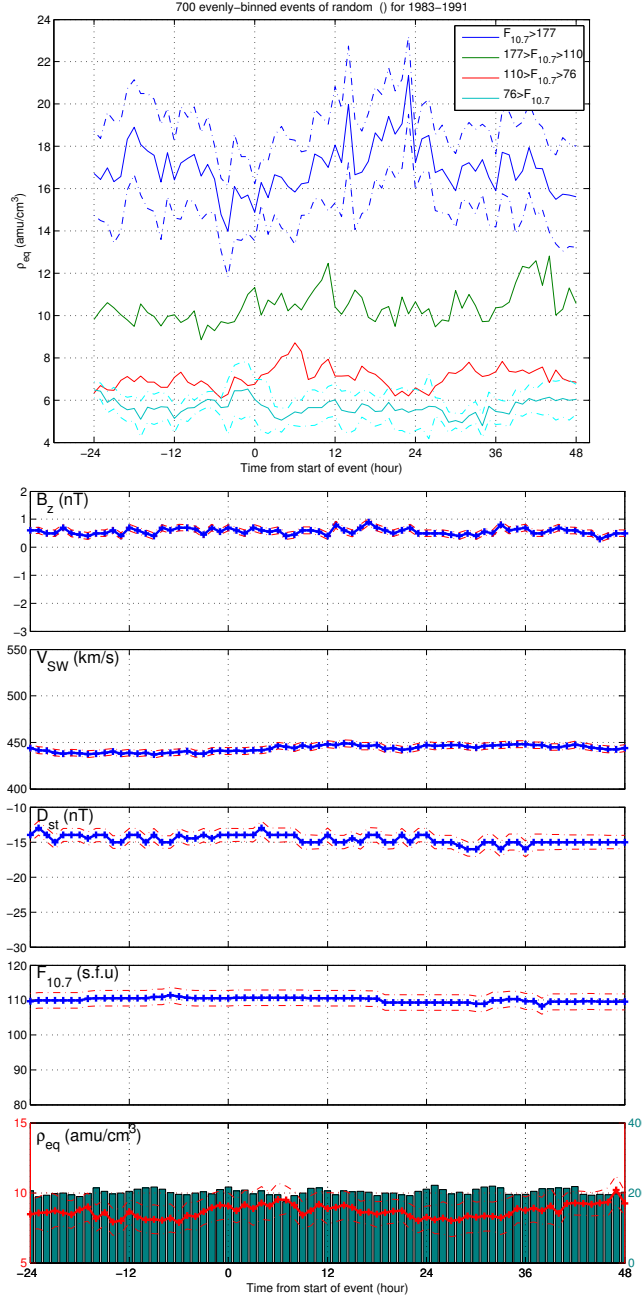


Figure 15: Top:  $\rho_{eq}$  binned by  $F_{10.7}$  for randomly selected times. Bottom: averages of randomly selected times

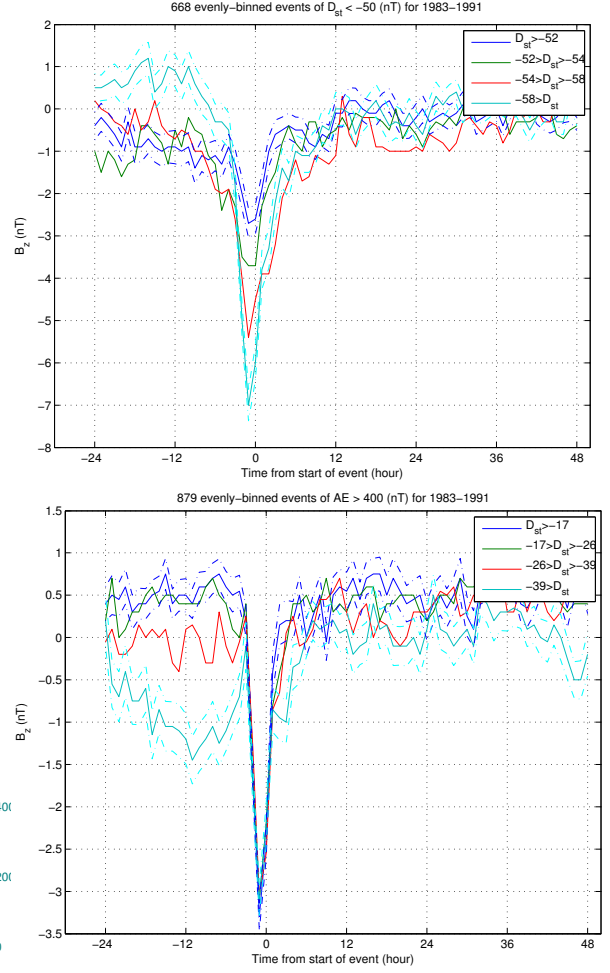


Figure 16: Top:  $B_z$  binned by  $D_{st}$  for  $D_{st} < -50$  nT events. Bottom:  $B_z$  binned by  $D_{st}$  for  $AE > 400$  nT events



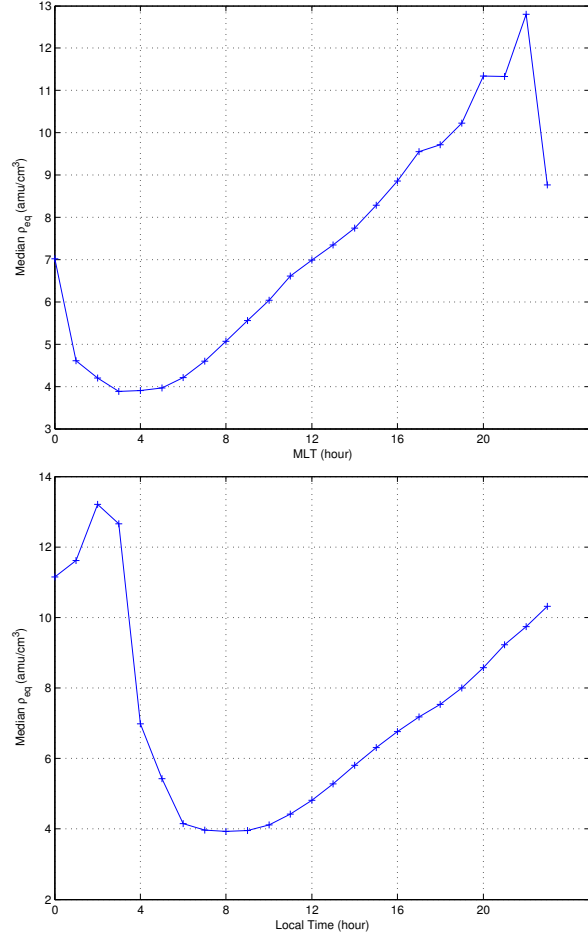


Figure 17: Median  $\rho_{eq}$  vs magnetic local time and universal time

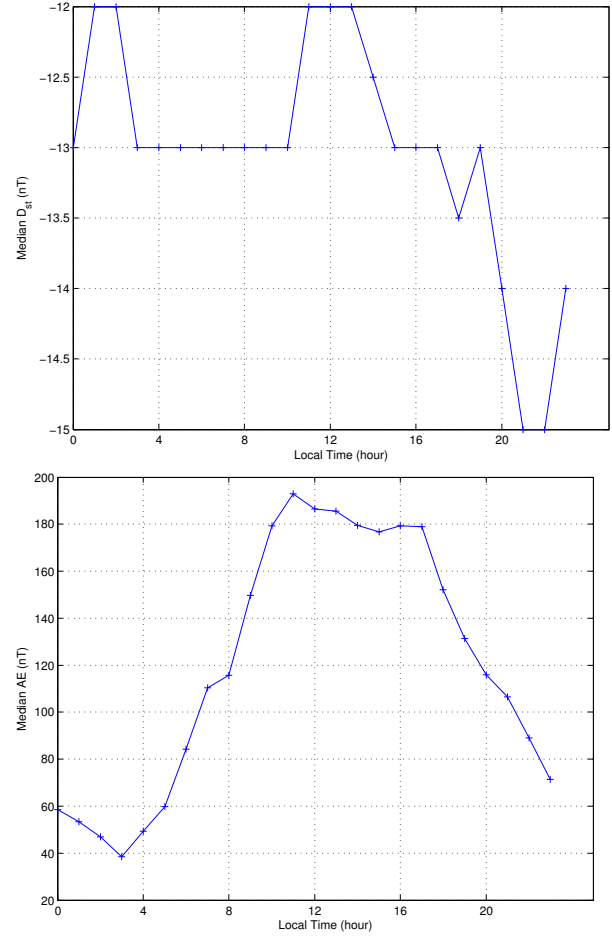


Figure 18: Median  $D_{st}$  vs universal time, and median AE vs universal time